CHAPTER 3. DESIGN AND ANALYSIS OF PHASE SHIFTER ELEMENTS

3.1. Introduction

The newly proposed coupler based phase shifter consists of three basic building blocks or elements, namely a splitter, tapered-line impedance transformers and a coupler. The function of the splitter is to divide the incoming signal into equal amplitude and phase vectors (or twins) and to transfer one of these signal parts to the other side of the middle slab of the tri-plate structure. A second splitter recombines the resultant equal phasors at the output of the device to conserve energy. The coupler combines the two vectors in such a way that the output vectors have a fixed amplitude ratio and quadrature difference. After vector addition, the phase shift depends on the coupling nature of the coupler. The function of the four $\sqrt{2}:1$ transformer tapers is to match the phase shifter input and output ports to the coupler. The transformers could be neglected if the input impedance level could be reduced to half the coupler internal impedance level. This is impractical, however, because the centre high-coupling-value section of the coupler will become too narrow to etch accurately. These elements will be analysed in detail to reveal the nature and limitations to the performance of the phase shifter. The results will also be used in the sensitivity and tolerance analysis, which will follow in Chapter 4.

First, the sensitivity of asymmetric spaced stripline devices is investigated. Then the tapered-line transformers are analysed and the sensitivity of exponential tapers to tolerance variations is calculated. The analysis and synthesis of stripline couplers then follows. Special attention is paid to the semi-distributed stripline splitter. First, broadside coupled stripline properties and the nature of the via interconnection is analysed with a full-wave analysis procedure. After that, the single and multiple-via splitting structure is analysed and the resonance properties are investigated. The *S*-parameters of the splitter is derived and practical considerations are discussed. The chapter ends with general conclusions.

3.2. Tapered Stripline Impedance Transformers

Before the tapered-line impedance transformer design is discussed it is essential to investigate the sensitivity of the conduction medium of this element to manufacturing tolerance. Therefore, the sensitivity of asymmetric spaced stripline devices is first discussed in paragraph 3.2.1. Then the tapered line transformer design is discussed in paragraph 3.2.2 and an investigation into the sensitivity of these tapers to manufacturing tolerances follows in paragraph 3.2.3.

3.2.1. Sensitivity of Asymmetric Spaced Stripline Structures

There is a need to know the effect of variation in some parameters in the characterization of the transmission structures, such as the 50 Ω lines and the 50 Ω - 100 Ω impedance transforming tapers of a phase shifter. It is assumed that the line and tapers are realised in asymmetric-spaced stripline conductors such as shown in Figure 12.

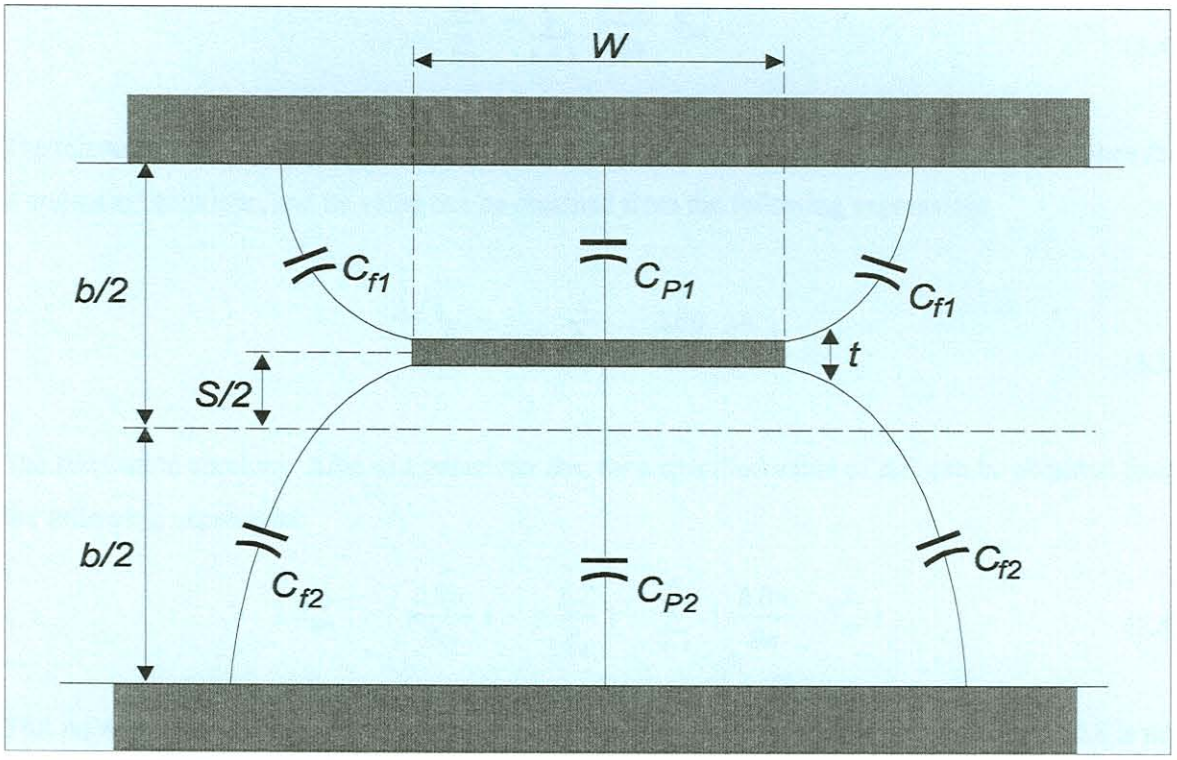

Figure 12 : Cross section of asymmetric spaced stripline devices

The normalized sensitivity of a function F with respect to a parameter x is defined as [1]

$$S_x^F = \lim_{\Delta x \to o} \frac{\Delta F/F}{\Delta x/x} , \tag{3.1}$$

$$= \frac{x}{F} \cdot \frac{\partial F}{\partial x} . \tag{3.2}$$

This is the ratio of the fractional change in the function F to the fractional change in the parameter x, referred to as the normalized sensitivity. The change in impedance ΔZ of a transmission line is related to the tolerance ΔB in parameter B by

$$\frac{\Delta Z}{Z_0} = \frac{\Delta B}{B} S_B^{Z_0} \quad , \tag{3.3}$$

where Z_0 is the impedance with ΔB equal to zero. When Z_0 is a function of several independent variables Bn, where $n = 1, 2 \ldots N$. The total change in Z_o is given by

$$\frac{\Delta Z}{Z_0} = \sum_{n=1}^{N} \frac{\Delta Bn}{Bn} S_{Bn}^{Z_0} \quad . \tag{3.4}$$

The tolerance ΔBn leads to a spread in value of ΔZ. The largest possible value of ΔZ determines the worst-case behaviour, and its value can be obtained from the following expression:

$$\frac{(\Delta Z)_{MAX}}{Z_0} = \pm \sum_{n=1}^{N} \left| \frac{\Delta Bn}{Bn} S_{Bn}^{Z_0} \right| \quad . \tag{3.5}$$

The fabrication accuracy ΔBm of a parameter Bm, for a specified value of ΔZ, can be obtained from the following expression:

$$\left| S_{Bm}^{Z_0} \right| \cdot \left| \frac{\Delta Bm}{Bm} \right| = \left| \frac{\Delta Z}{Z_0} \right| - \sum_{n \neq 1}^{N} \left| \frac{\Delta Bn}{Bn} \cdot S_{Bn}^{Z_0} \right| \quad . \tag{3.6}$$

This equation holds when the right-hand side is positive, otherwise the specified value of ΔZ is not realisable with the given set of ΔBn values. This analysis is useful in determining the trade-off between the tolerances and the performances. Before calculating the sensitivities of asymmetric spaced stripline structures, the impedance properties of these structures are reviewed. The impedance of asymmetric spaced stripline devices can be stated as follows (see Figure 12) [2]

$$Z_0 = \frac{120\pi}{\sqrt{\epsilon_r}} \cdot \frac{1}{C/\epsilon} \quad , \tag{3.7}$$

where

$$C/\epsilon = C_{P1}/\epsilon + C_{P2}/\epsilon + 2\, C_{f1}/\epsilon + 2\, C_{f2}/\epsilon \quad . \tag{3.8}$$

The total conductor unit-length capacitance C/ϵ is comprised of plate capacitances C_{P1}/ϵ and C_{P2}/ϵ and the fringe fields C_{f1}/ϵ and C_{f2}/ϵ. The fringe fields can be calculated from

$$C_{fi}/\epsilon = \frac{1}{\pi}\left[2\,\xi_i \ln(\xi_i + 1) - (\xi_i - 1)\ln(\xi_i^{\,2} - 1)\right] , \tag{3.9}$$

where

$$\xi_1 = \frac{1}{1 - \dfrac{t}{b - s}} , \tag{3.10}$$

and

$$\xi_2 = \frac{1}{1 - \dfrac{t}{b + s}} . \tag{3.11}$$

The plate capacitances can be calculated from the following equations:

$$C_{P1}/\epsilon = \frac{\dfrac{2w}{b - s}}{1 - \dfrac{t}{b - s}} , \tag{3.12}$$

and

$$C_{P2}/\epsilon = \frac{\dfrac{2w}{b + s}}{1 - \dfrac{t}{b + s}} . \tag{3.13}$$

For symmetric spaced stripline devices, the equation for Z_0 simplifies to

$$Z_0 = \frac{120\pi}{\sqrt{\epsilon_r}}\left[\frac{w}{b - t} + C_f/\epsilon\right]^{-1} , \tag{3.14}$$

and

$$C_f/\epsilon \fallingdotseq \frac{\ln(4)}{\pi} \qquad \text{for } t \ll b . \tag{3.15}$$

According to Getsinger [3], the width must be compensated for the loss of fringe field capacitances when

$$\frac{w}{b - t} \leq 0.35 . \tag{3.16}$$

The new width must become

$$w'/b = \frac{1}{1.2}\left[0.07\left(1 - \frac{t}{b}\right) + \frac{w}{b}\right] . \tag{3.17}$$

In a typical case where 5 mil substrate is sandwiched between two 20 mil substrates, this compensation adds 1 μm at 75Ω ($\pm$ 0. 4 mm) and gradually increases to a maximum of 50 μm where w approaches 0 (infinite impedance line). Since the effects of compensation is negligible in the tolerance analysis, it is neglected. The sensitivity of Z_0 with respect to $x = w, b, s, t$ and ϵ_r, may be calculated as follows:

$$S_x^{Z_0} = \frac{x}{Z_0} \cdot \frac{\partial Z_0}{\partial x} \quad , \tag{3.18}$$

$$= \frac{x}{120\pi} \cdot \sqrt{\epsilon_r} \cdot C/\epsilon \cdot \frac{\partial Z_0}{\partial x} \quad . \tag{3.19}$$

If $x = \epsilon_r$ then the sensitivity of the line impedance to the dielectric constant ϵ_r becomes

$$S_{\epsilon_r}^{Z_0} = -\,½ \quad \text{since} \quad \frac{\partial}{\partial \epsilon_r}\left[C/\epsilon \right] = 0 \quad . \tag{3.20}$$

If $x = w, b, s, t$ then we calculate (3.18) as

$$S_x^{Z_0} = \frac{-x}{C/\epsilon} \cdot \frac{\partial}{\partial x}\left[C/\epsilon \right] \quad . \tag{3.21}$$

Substituting equation 3.7 into 3.21, it is found that

$$S_x^{Z_0} = \frac{-xZ_0\sqrt{\epsilon_r}}{120\pi} \cdot \frac{\delta}{\delta x}\left[C/\epsilon \right] \quad . \tag{3.22}$$

From the definition of tolerance analysis in equation (3.3), it follows that

$$\Delta Z_0 = \Delta x \cdot \left[S_x^{Z_0} \cdot \frac{Z_0}{x} \right] \quad . \tag{3.23}$$

Equation 3.22 can be expanded to yield the following sensitivity equation:

$$S_x^{Z_0} = \frac{-x}{C/\epsilon}\left[\frac{\partial}{\partial x} C_{P1}/\epsilon + \frac{\partial}{\partial x} C_{P2}/\epsilon + 2\,\frac{\partial}{\partial x} C_{f1}/\epsilon + 2\,\frac{\delta}{\delta x} C_{f2}/\epsilon \right] \quad . \tag{3.24}$$

The following constants are defined, to simplify the expressions for the sensitivity analysis

$$A = \frac{1}{b - s - t} \qquad B = \frac{1}{b + s - t} \quad , \tag{3.25}$$

$$M = \frac{2/\pi}{(b - s - t)^2} \ln\left[2\left(\frac{b - s}{t}\right) - 1\right] \quad , \tag{3.26}$$

$$N = \frac{2/\pi}{(b + s - t)^2} \ln\left[2\left(\frac{b + s}{t}\right) - 1\right] \quad , \tag{3.27}$$

$$X = C_{f1}/\epsilon + C_{f2}/\epsilon \quad . \tag{3.28}$$

The sensitivity of the line impedance to the various parameters are then calculated as

$$S_{\epsilon_r}^{Z_0} = -\tfrac{1}{2} \quad , \tag{3.29}$$

$$S_t^{Z_0} = \frac{-t}{C/\epsilon} \cdot \left[2w\,(A^2 + B^2) + (b - s)\,M + (b + s)\,N\right] \quad , \tag{3.30}$$

$$S_w^{Z_0} = \frac{-2w}{C/\epsilon} \cdot \left[A + B\right] \quad , \tag{3.31}$$

$$S_s^{Z_0} = \frac{-s}{C/\epsilon} \cdot \left[2w\,(A^2 - B^2) + t\,(M - N)\right] \quad , \tag{3.32}$$

$$S_b^{Z_0} = \frac{-b}{C/\epsilon} \cdot \left[-2w\,(A^2 + B^2) - t\,(M + N)\right] \quad , \tag{3.33}$$

where

$$\frac{1}{C/\epsilon} = \frac{\sqrt{\epsilon_r}\,Z_0}{120\pi} \quad , \tag{3.34}$$

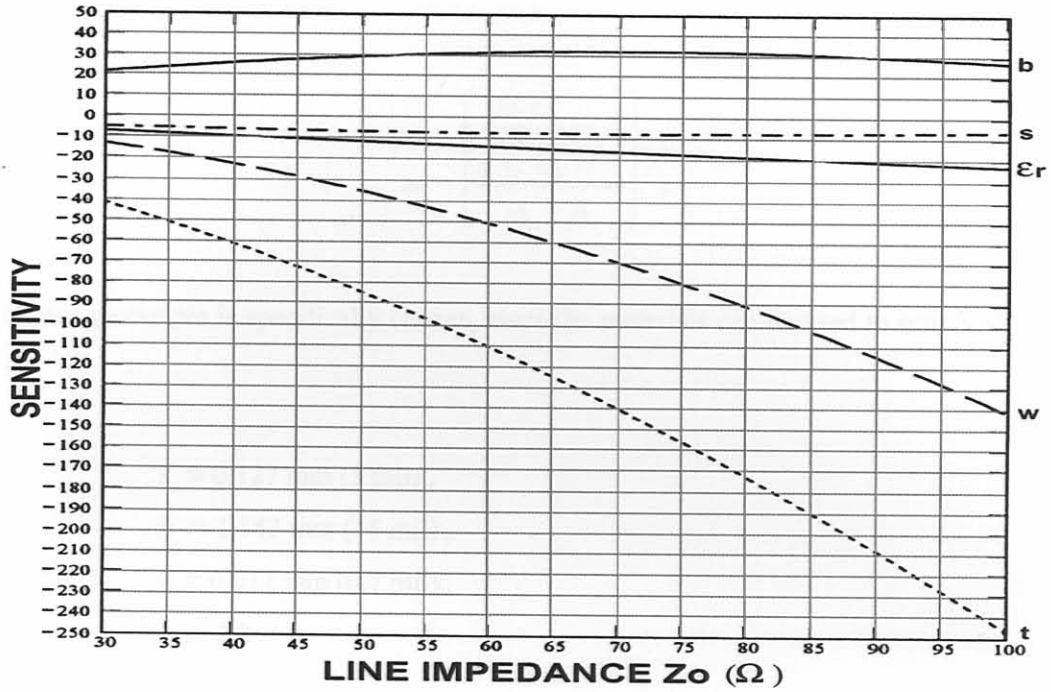

Figure 13 : Sensitivity of asymmetric spaced stripline

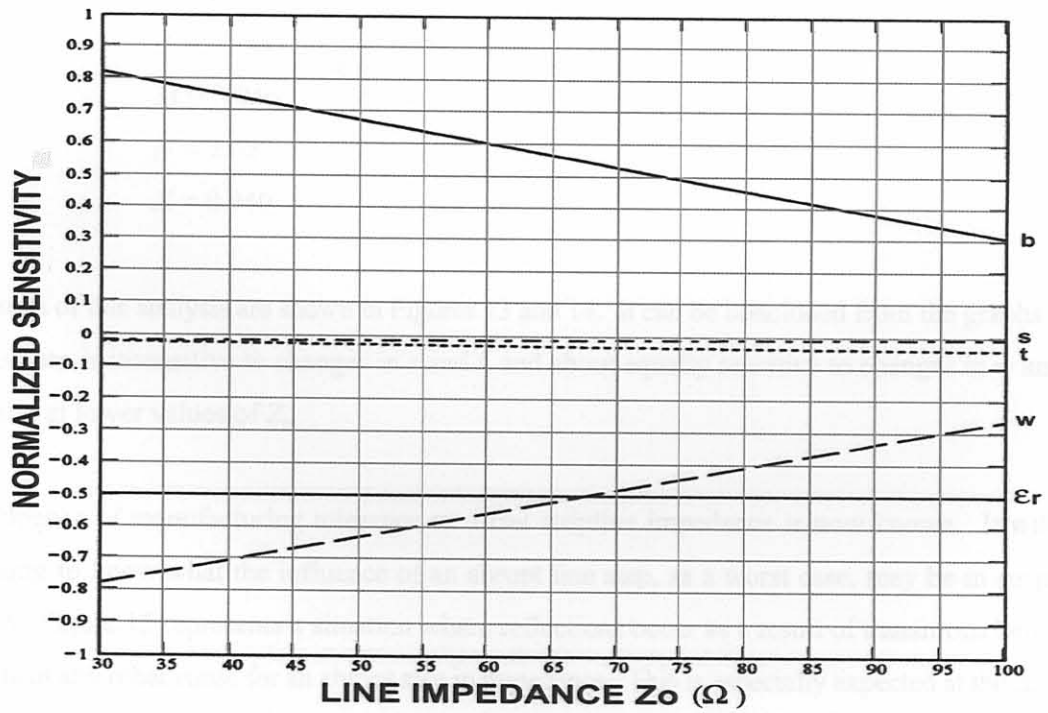

Figure 14 : Normalized sensitivity of asymmetric spaced stripline

and

$$w = \left[\frac{\frac{60\pi}{\sqrt{\epsilon_r}\, Z_0} - X}{A + B} \right] . \tag{3.35}$$

The following example is specifically chosen, since the materials can be used to satisfy almost all designs:

$s = 0.127$ mm (5 mil),
$b = 1.143$ mm (45 mil),
$t = 0.017$ mm (0.7 mil),
$\epsilon_r = 2.2$.

The previously defined constants, equations (3.25) - (3.28) are then:

$A = 1.001$
$B = 0.798$
$M = 3.046$
$N = 2.027$
$X = 0.940$

The results of this analysis are shown in Figures 13 and 14. It can be concluded from the graphs that the structure is insensitive to changes in s and t, and about equally sensitive to changes in w and b, especially at lower values of Z_0.

The influence of manufacturing tolerance to offset stripline impedance is now known. It will be interesting to know what the influence of an abrupt line step, as a worst case, may be in stripline medium. Figure 15 represents a situation where reflections occur as a result of transitions between elements or any other cause for an abrupt step in impedance. This is especially expected at the splitter ports, since the impedance tapers can be connected to the couplers in a smooth transition.

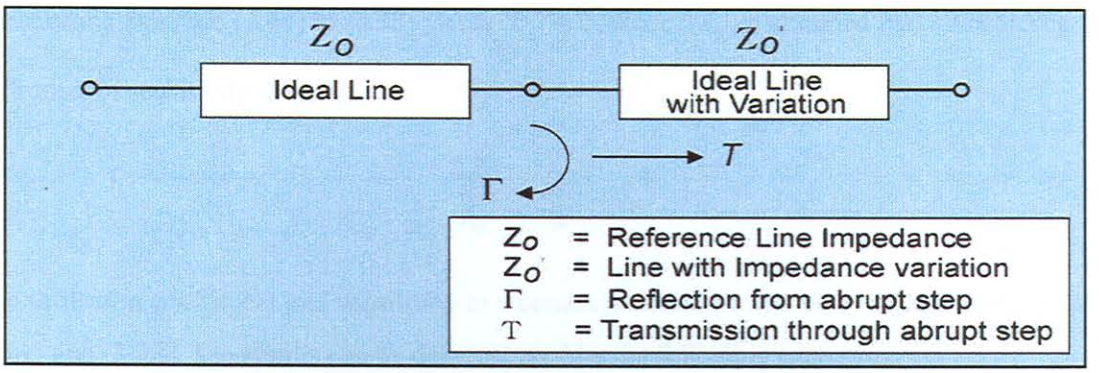

Figure 15 : Reflections due to an abrupt impedance step

Let the reflection and transmission coefficients be defined as

$$\Gamma = \frac{Z_0' - Z_0}{Z_0' + Z_0} \quad , \tag{3.36}$$

$$T = 1 + \Gamma = \frac{2\,Z_0'}{Z_0' + Z_0} \quad . \tag{3.37}$$

The error vector can be described as

$$V_e\, e^{j\Psi e} = T - 1 = \Gamma \quad . \tag{3.38}$$

Substituting (3.36) into (3.38) yields

$$V_e\, e^{j\Psi e} = \frac{Z_0' - Z_0}{Z_0' + Z_0} \quad , \tag{3.39}$$

where

$$Z_0' = Z_0 + \Delta Z_0 \quad . \tag{3.40}$$

Therefore, substituting (3.40) in (3.36) and simplifying, yields

$$\Gamma = \frac{\left(\frac{\Delta Z_0}{Z_0}\right)}{2 + \left(\frac{\Delta Z_0}{Z_0}\right)} \quad . \tag{3.41}$$

Substituting equation (3.41) in (3.38) yields $\Psi_e = 0$, since ΔZ_0 is assumed real. According to the definition of sensitivity in (3.3),

$$\frac{\Delta Z_0}{Z_0} = \frac{\Delta x}{x} \cdot S_x^{Z_0} \quad . \tag{3.42}$$

The reflection coefficient and sensitivity to a certain parameter x can be evaluated using equations (3.41) and (3.42). The results can be demonstrated by the following examples:

- A change of 10% in the ϵ_r parameter causes a -33 dB reflection coefficient, independent of Z_0.
- A change of 10μm in t causes a -38 dB reflection for 100 Ω lines, and -44 dB reflection for 30 Ω lines.
- A change of +0.2 mm in w causes a -15 dB reflection for 100 Ω lines and -28 dB reflection for 30 Ω lines. A negative change in w provides a slightly better situation.
- A change of 0.05 mm in s causes a -48 dB reflection for 30 Ω lines and -57 dB for 100Ω lines.
- A change of 0.1 mm in b causes a -29 dB reflection for 30 Ω lines and a -38 dB reflection or 100 Ω lines.

3.2.2. Tapered-Line Transformer Design

We now present the design of the tapered-line impedance transformers. The reflection coefficient from any tapered line, assuming small internal reflections, can be described by the following integral [4]:

$$\Gamma = \tfrac{1}{2} \int_0^L e^{-j2\beta z} \cdot \frac{d}{dz} (\ln Z)\, dz \quad . \tag{3.43}$$

where L represents the taper length, z the distance variable along the taper, and Z the taper impedance as a function of z. The best choice of taper would be the well-known Klopfenstein taper [5], since it has a minimum equal ripple reflection coefficient magnitude in the pass band for a specified taper length. RP Hecken [6] offers design procedures for a "near-optimum" taper, which avoids the small impedance steps required by the optimum taper at the ends of the taper. These steps could possibly add asymmetric parasitic components at the coupler inputs, and should be avoided.

To relieve the phase shifter designer of time-consuming taper synthesis, the straight-forward exponential taper is recommended. In an exponential taper the impedance is tapered in an exponential fashion along the length of the device. This also considerably simplifies the sensitivity and tolerance analyses of the taper. Due to internal reflections, a tapered line is not entirely dispersionless. However, test results in chapter 5 suggest that this effect is small enough to approximate linear behaviour and allow compensation via the reference line. For exponential tapers, the normalized impedance takes the form

$$Z(z) = \alpha^{z/L} \qquad \text{where} \qquad \alpha = Z_2/Z_1 \ . \tag{3.44}$$

Substitution in the integral (3.43), and simplification yields

$$\Gamma = \tfrac{1}{2}\, e^{-j\beta L} \cdot \ln \alpha \cdot \left[\frac{\sin(\beta L)}{\beta L}\right] \ . \tag{3.45}$$

For a 50-100 Ω taper, equation (3.45) yields

$$|\Gamma|\,(dB) = 20 \log\left[\ln\sqrt{2} \cdot \frac{\sin(\pi x)}{\pi x}\right] , \tag{3.46}$$

where

$$x = \frac{2L}{\lambda} \ . \tag{3.47}$$

The theoretical reflection minima occur where $\beta L = n\pi$ ($n = 1, 2, 3 \ldots$), and maxima where $\beta L = 0$ and $\beta L = m$ ($m = 3, 5, 7 \ldots$). The maximum reflection occurs (out of band) at 0GHz and is theoretically -9.2dBc. The maximum in-band reflection occurs at 3GHz and is expected to be -22.6dBc, as seen in Figure 16.

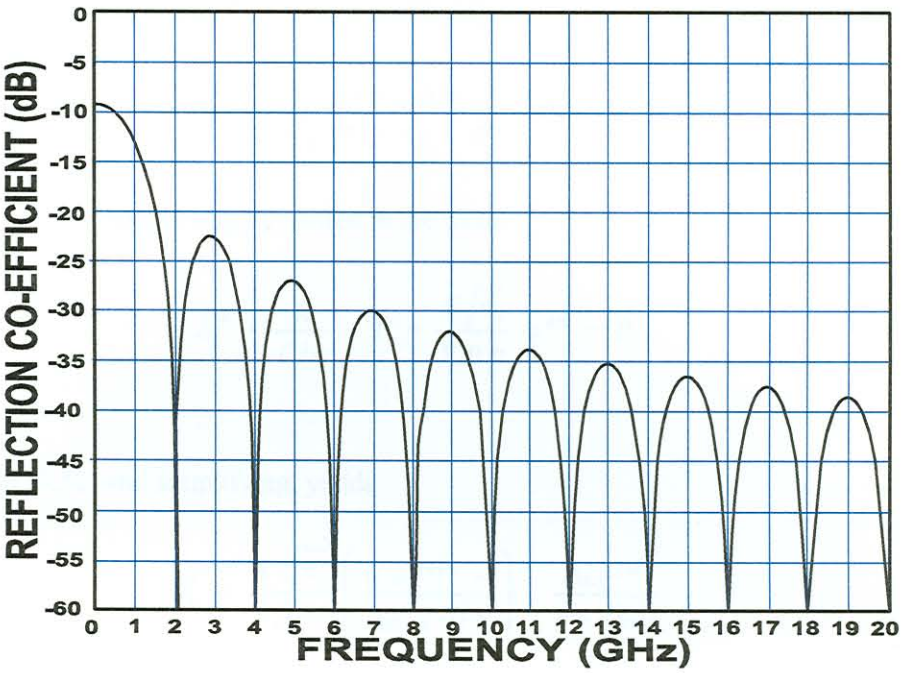

Figure 16 : Impedance taper theoretical reflection coefficient

It can be concluded therefore that the reflection maxima is exceptionally low, even at the highest in-band lobe (lobe #2). The taper length can be related to lower cutoff frequency as

$$L\ (f_L) = \frac{\lambda_L}{2} = \frac{C}{2\sqrt{\epsilon_r}\, f_L} \quad , \tag{3.48}$$

$$L = \frac{150}{\sqrt{\epsilon_r}\, f_L} \quad . \tag{3.49}$$

where the length is in millimetres and the frequency in Gigahertz.

3.2.3. The Sensitivity of Exponential Tapers

The theory can be extended to calculate the sensitivity of the impedance transforming tapers to material and manufacturing tolerance. Using the mathematical description of the reflection coefficient of a taper in general, and the definition of sensitivity for Γ with respect to any parameter x,

$$S_x^{\Gamma} = \frac{x}{\Gamma_0} \cdot \frac{\partial \Gamma}{\partial x} \quad . \tag{3.50}$$

Then, after substituting in equation (3.43) and simplifying, yields

$$S_x^{\Gamma} = \frac{x}{2\Gamma_0} \int_0^{L} e^{-j2\beta z} \frac{\partial}{\partial z} \left(S_x^{z} \right) dz \quad . \tag{3.51}$$

The sensitivity of impedance can be written in the form

$$S_x^{z} = \frac{K}{C/\epsilon} + P = \frac{K\sqrt{\epsilon_r}}{120\,\pi}\, \alpha^{\,z/L} + P \quad . \tag{3.52}$$

Substitution in (3.51) and simplifying, yields

$$S_x^{\Gamma} = \frac{K\sqrt{\epsilon_r}}{120\,\pi} \left(\frac{\alpha\, e^{-j2\beta L} - 1}{\ln \alpha^{\,j2\beta L}} \right) \cdot \frac{\beta L e^{j\beta L}}{\sin(\beta L)} \quad , \tag{3.53}$$

where α represents the impedance ratio of the taper. If $\alpha = 2$ (50 Ω - 100 Ω taper) and $2\beta L > \ln \alpha$ (in the passband) then

$$S_x^{\Gamma} \simeq \frac{K\sqrt{\epsilon_r}}{240\,\pi} (3 + j \cot \beta L) \quad . \tag{3.54}$$

To find the frequency βL at which S_x^{Γ} is maximum, we solve for

$$\frac{\partial \mid S_x^{\Gamma} \mid}{\partial (\beta L)} = 0 \quad . \tag{3.55}$$

Therefore

$$\beta L = \pm n\pi; \qquad n = 0, 1, 2 \ldots \tag{3.56}$$

i.e. in the dips (minima) of Γ. The peaks of Γ occur at:

$$\beta L = \frac{\pi}{2} \pm n\pi; \quad n = 0, 1, 2 \ldots \tag{3.57}$$

The first lobe of Γ is the maximum, where

$$\beta L = \frac{3\pi}{2} \quad . \tag{3.58}$$

This is therefore where the maximum influence of tolerance variations is expected. Therefore

$$S_x^{\Gamma}\,/_{\beta L = \frac{3\pi}{2}} = \frac{K\sqrt{\epsilon_r}}{80\pi} \quad . \tag{3.59}$$

Now

$$\Gamma_{New} = \Gamma_0 + \Delta\,\Gamma \quad , \tag{3.60}$$

$$= \Gamma_0 \left[1 + \frac{\Delta x}{x}\, S_x^{\Gamma}\right] \quad . \tag{3.61}$$

The maximum reflection from the impedance taper transformer due to manufacturing tolerance is therefore

$$|\,\Gamma_{MAX}\,| = \frac{ln2}{3\pi}\left[1 + \frac{\Delta x}{x} \cdot \frac{K\sqrt{\epsilon_r}}{80\pi}\right] \quad . \tag{3.62}$$

Substituting equation (3.52) in (3.29) to (3.33) and solving for the value of K, it can be shown that

$$K_{\epsilon_r} = 0 \quad , \tag{3.63}$$

$$K_t = 2X\,t\,\frac{(A^2 + B^2)}{A + B} - t\,[\,(b - s)\,M + (b + s)\,N] \quad , \tag{3.64}$$

$$K_w = 2X \quad , \tag{3.65}$$

$$K_s = 2sX\,(A - B) - ts\,(M - N) \quad , \tag{3.66}$$

$$K_b = -2bX\,\frac{(A^2 + B^2)}{A + B} + bt\,(M + N) \quad , \tag{3.67}$$

where the constants A, B, M, N and X are as defined before in equations (3.25) - (3.28). This analysis infers the following:

- A perfect taper has a first in-band lobe reflection of -22.68 dB.
- A worst case taper reflection of -22.6 dB is expected for a combined tolerance of 10% on parameters w, b, s, t or ϵ_r .

- The taper is most sensitive to variations in parameters t and w.
- The taper is not sensitive to material or manufacturing tolerances.

3.3. Stripline Coupler Design and Practical Considerations

3.3.1. Analysis and Synthesis of Stripline Couplers

Coupler design tables were presented by Crystal and Young in 1965 [7]. Equal-ripple polynomials were determined and applied to the synthesis of symmetric TEM-mode coupled transmission line directional couplers using exact analysis. The tables of symmetric couplers of various nominal coupling values over a range of ripple and bandwidths were published. An optimization program was written to iteratively derive the impedances of any number of section couplers over any specific bandwidth and equal-ripple value. Using the tables published by Crystal and Young, or the optimization program, a coupler with arbitrary specification can be synthesized.

When such a multi-section coupler is implemented, Tresselt found that the spread in coupling values required in adjacent quarter-wave sections is large enough to produce substantial differences in physical line dimensions [8]. Furthermore, a finite length of transition is required to realise these junctions. These transitions then excite higher order modes which can be represented by reactive parasitic components. The effects of these parasitic elements are especially noticeable at higher frequencies where VSWR and directivity are degraded.

Tresselt wrote a paper [8] in 1966 on the synthesis and design of high-directivity 90° couplers using non-uniform line techniques. The design employs a continuously-tapered coupling coefficient, resulting in a nonuniform coupler having optimum bandwidth for a given coupler length. It is interesting to note that these nonuniform couplers are a quarter-wavelength longer at centre frequency than the stepped equivalent prototype, and requires a somewhat tighter maximum coupling coefficient at the coupler centre. In effect, the Tresselt procedure provides a means of smoothing out a discrete section coupler. Kammler [9] demonstrated that the Tresselt procedure does not always give rise to the optimal continuously tapered coupler. Kammler presented a computer-aided design procedure employing a special optimization process to produce the optimum coupling response. Standard

parametric forms based on an approximate Fourier analysis as well as a more general spline parametric form were developed and illustrated. He could, however, only demonstrate very small differences between his optimal design and the Tresselt procedure.

The author of this thesis used Tresselt's design procedure to design several couplers, and very good practical results were obtained. Shelton's paper [10] on impedances of offset parallel-coupled strip transmission lines were used continuously to calculate physical line dimensions of the tapered lines. The assumption was made (and proved valid) that the non-uniform line couplers taper so gradual, that it permits usage of physical coupling data based on infinitely long, uniformly-coupled line calculations.

After confidence was gained in the analysis and synthesis of these couplers, a program was compiled to automate all the labourious calculations. The number of sections, coupling, triplate dimensions and permittivity are specified along with the centre frequency. The program calculates the coupling required at the centre of the coupler where the coupler is completely over-coupled, i.e. the lines are broadside coupled. The line dimensions are calculated to satisfy the coupling value and to approach the 50 Ω system impedance as closely as possible. The impedance, defined as the square root of the product of the even - and odd - mode impedances, is usually within 5 Ω from the system impedance at the input of the coupler. The coupler impedance is then tapered in a linear fashion from the centre impedance value to the 50 Ω system impedance at the input of the coupler. This impedance taper, along with the coupling taper, is used as input to the program section which calculates the taper of the physical dimensions of the coupler. The program produces a text file with the coupling, even and odd mode impedances, and line width and offset as a function of distance, in tabular form. It also creates an AutoCad-format graphical file which can be used to generate the photolithographic mask needed to etch the coupler.

A 5-section coupler was designed with the aid of the program, and practically evaluated. The designed physical taper was then divided into 100 incremental sections, each with an average line width and coupling offset. The *S*-parameters of each incremental section was evaluated by two different methods; Shelton's closed-form equations, and a full-wave FEM analysis computer program. The *S*-parameter files were cascaded and the theoretical performance of the coupler was analysed and evaluated. The results were so closely matched that no difference was visible on overlay graphs up to 18GHz. The frequency behaviour of a typical 9-section test coupler is shown in Appendix E.

3.3.2. Tolerance Analysis of Stripline Couplers

The sensitivity and tolerance analysis of a single-section coupler is described in detail by Srigiripuram et al. [11]. Since mathematical equations describing the sensitivity and tolerance of multi-section couplers is a complex issue worthy of an entire separate treatise, the analysis is simplified by dividing it into a material tolerance analysis and an etching alignment analysis.

The dual, tandem-connected 3dB coupler is divided into a large amount of equal-length sections. A single parameter of these sections is then independently randomly adjusted within certain tolerances and the coupling and phase responses of the coupler are optimized for worst performance. To avoid the publication of numerous results, the worst case numbers are recorded and summarized in Table 3.1.

- Over- and Under-Etching

All line widths were simultaneously adjusted by up to twice the tolerance of over- or under-etching. All other parameters were fixed. For a tolerance of 25 micron, a 0.45 dB coupling deviation was observed. Since the structure remained symmetric, no phase distortion was recorded. The bandwidth of the coupler remained unchanged (See Table 3.1).

- Photolithography Scaling Errors

All layout dimensions such as lengths, widths and offsets, were scaled by fixed percentages. For a -5% scaling tolerance, a 0.48 dB coupling deviation was recorded, and for a +5% scaling tolerance, a 0.15 dB coupling deviation was recorded. Since the structure remained symmetric, no phase distortion occurred. In general, amplitude distortion was worse at higher frequencies. The bandwidth also changed with the same percentage as the scaling error (Table 3.1).

- Mask Alignment Errors

The etching masks can be misaligned in three ways. When a small misalignment occurs in the direction of the length of the coupling sections, only negligible errors are caused. When the misalignment occurs in the direction transverse to the length of the coupled sections, the effect is that

of moving the over-coupled area of the coupler to one side, increasing the coupling of all sections to that side, and decreasing the coupling of all sections on the opposite side. For a 70 μm misalignment error, errors of 0.6 dB in coupling and 5.6° in phase were recorded. The bandwidth of the coupler remained unchanged.

- Rotational Alignment Errors

When one etch mask is rotated with respect to the other by 3.5°, 12.5 dB of coupling error and 7° of phase distortion are caused. For a 1° rotational misalignment, errors of 0.8 dB in coupling and 0.3° in phase were recorded. The bandwidth was virtually unaffected (Table 3.1).

- Material Tolerances

The analysis results for certain parameter tolerances are summarized in Table 3.1. ($\mathcal{P}$ is a scaling factor of the resistivity of the cladding material relative to copper):

Table 3.1 : Effect of material tolerances on couplers

Parameter	Tolerance	δC (dB)	ΔP (deg)	ΔBandwidth
s	±10 μm	0.55	-	-
b	+100/-100 μm	0.4/0.25	-	+0.4 GHz./-0.5GHz
t	±15 μm	0.01	-	-
ϵ_r	+20% / -20%	-	-	-1.6 GHz./+2 GHz
ρ	+100% / -100%	-	0.12/0.25	-
Roughness	±10 μm	0.18	3.9	-

Regarding the tolerance analyses of stripline couplers, the following conclusions can be summarized:

- Symmetric couplers have no phase balance distortion. Material tolerances do not influence phase behaviour.
- Over- or under-etching and scaling errors also does not influence phase behaviour.

- Coupler amplitude and phase response are very sensitive to alignment, especially rotational errors.

- Amplitude behaviour is sensitive to virtually all errors, especially variations in s. Measured values should be used in design, as supplier tolerance is typically 12 μm.

- Phase and amplitude response are very sensitive to random surface errors, or roughness.

3.4. Semi-Distributed Stripline Splitter

3.4.1. Introduction

The function of the splitter is to divide an incoming signal into two signal twins, very closely matched in amplitude, and especially phase. Likewise, it must also recombine two signal twins into a single output signal. The symmetric stripline coupler utilized in the phase shifter has its input ports on opposite sides of the centre dielectric slab of the triplate structure. This complicates the splitter to the extent that the divided signals must also appear on opposite sides of the triplate structure, to enter the coupler. The same geometrical problem occurs at the output of the coupler, where recombination of the signal twins occurs.

An ideal splitter is presented in Figure 17. If one of the splitter output signals is routed to the other side of the substrate, the symmetry is destroyed. The interconnection via introduces a series inductance which cannot be avoided. After much consideration, many experiments and simulations, the semi-distributed stripline splitter was developed [12]. The properties of an ideal splitter are now derived, after which the semi-distributed splitter is introduced.

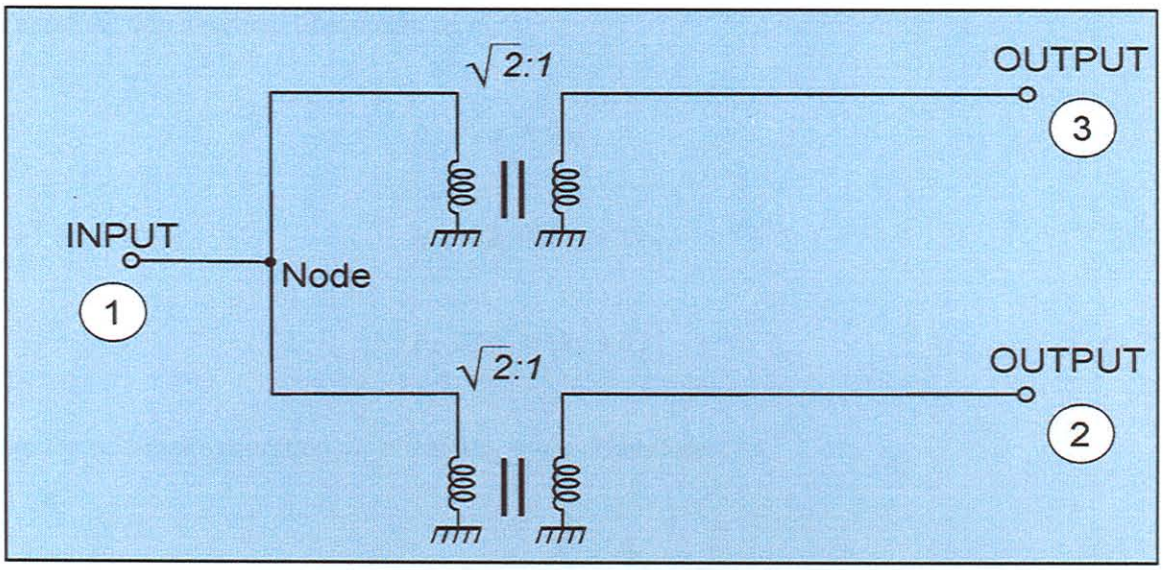

Figure 17 : The ideal splitter schematic

The three port splitter *S*-parameter matrix can be represented as

$$[S] = \begin{bmatrix} S_{11} & S_{12} & S_{13} \\ S_{21} & S_{22} & S_{23} \\ S_{31} & S_{32} & S_{33} \end{bmatrix} . \tag{3.68}$$

Let

$$T = S_{21} = S_{12} = S_{31} = S_{13} \quad \text{(Equal Split)} , \tag{3.69}$$

$$\Gamma = S_{22} = S_{33} \quad \text{(Output Match)} , \tag{3.70}$$

$$C = S_{23} = S_{32} \quad \text{(Isolation)} . \tag{3.71}$$

If the input port is matched at all conditions, the *S*-parameter matrix can be simplified to

$$[S] = \begin{bmatrix} 0 & T & T \\ T & \Gamma & C \\ T & C & \Gamma \end{bmatrix} . \tag{3.72}$$

Therefore, when written in equation form,

$$b_1 = Ta_2 + Ta_3 , \tag{3.73}$$

$$b_2 = Ta_1 + \Gamma a_2 + Ca_3 , \tag{3.74}$$

$$b_3 = Ta_1 + Ca_2 + \Gamma a_3 . \tag{3.75}$$

For the odd-mode condition, $a_1 = 0$ and $a_2 = -a_3$. Therefore

$$b_1 = 0; \qquad \frac{b_2}{a_2} = \frac{b_3}{a_3} = \Gamma - C \quad . \tag{3.76}$$

The odd-mode reflection and transmission coefficients can therefore be defined as

$$\rho_0 = \Gamma - C \qquad \text{(Reflection)} , \tag{3.77}$$

$$\tau_0 = 0 \qquad \text{(Transmission)} . \tag{3.78}$$

For the even-mode condition, $a_1 = 0$ and $a_2 = a_3$. Therefore

$$b_1 = 2\ Ta_2 \quad , \tag{3.79}$$

$$\frac{b_2}{a_2} = \frac{b_3}{a_3} = \Gamma + C \quad , \tag{3.80}$$

$$\frac{b_1}{a_2} = 2T \quad . \tag{3.81}$$

The even-mode refection and transmission coefficients can therefore be defined as

$$\rho_e = \Gamma + C \qquad \text{(Reflection)} , \tag{3.82}$$

$$\tau_e = 2T \qquad \text{(Transmission)} . \tag{3.83}$$

Solving for the unknown *S*-parameters, yields

$$\Gamma = \frac{\rho_e + \rho_o}{2} \quad , \tag{3.84}$$

$$C = \frac{\rho_e - \rho_o}{2} \quad , \tag{3.85}$$

$$T = \frac{\tau_e}{2} \quad . \tag{3.86}$$

But

$$\tau_e = \sqrt{2} \qquad \text{(lossless combination of ports 2 \& 3)} \, , \tag{3.87}$$

$$\rho_0 = \frac{0 - Z_0}{0 + Z_0} = -1 \qquad \text{(virtual short circuit at node)} \, , \tag{3.88}$$

$$\rho_e = 0 \qquad \text{(all ports matched in even mode)} \, . \tag{3.89}$$

$$\therefore \ \Gamma = -1/2 \quad , \tag{3.90}$$

$$C = 1/2 \quad , \tag{3.91}$$

$$T = 1/\sqrt{2} \quad . \tag{3.92}$$

Assuming a transmission phase angle θ, the ideal phase shifter splitter *S*-parameter matrix can therefore be represented by

$$[S] = \begin{bmatrix} 0 & \frac{1}{\sqrt{2}} e^{-j\theta} & \frac{1}{\sqrt{2}} e^{-j\theta} \\ \frac{1}{\sqrt{2}} e^{-j\theta} & -1/2 e^{-j2\theta} & 1/2 e^{-j2\theta} \\ \frac{1}{\sqrt{2}} e^{1j\theta} & 1/2 e^{-j2\theta} & -1/2 e^{-j2\theta} \end{bmatrix} . \tag{3.93}$$

After much consideration, it was realised that an electrically short splitter will always add a phase lag to the signal split off to the other side of the centre slab of the practical triplate structure. This is due to the extra physical path length added by the interconnecting via, or any other interconnecting device. The solution was to use a semi distributed splitter, consisting of a length of broadside coupled stripline (BCS) structure with a number of interconnecting vias to distribute the split over an electrically longer structure, as shown in Figure 18.

To simplify the analysis, the vias are chosen to be of identical diameter and equal spacing. The via diameter is also chosen to be small compared to the BCS width, in order to prevent even-mode fringe field disturbance. In the even mode, the overlapping lines of the BCS structure are excited in phase, and out of phase in the odd mode.

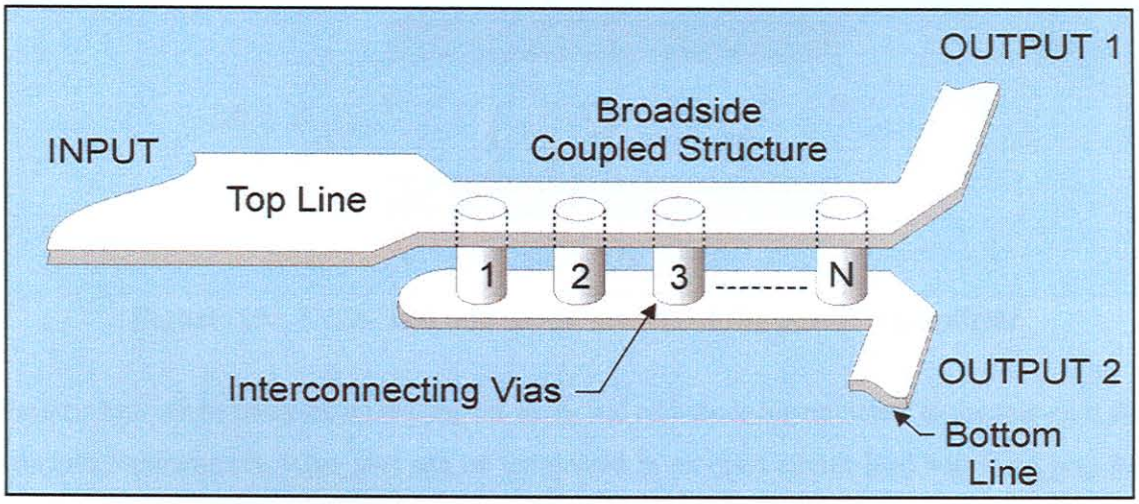

Figure 18 : The semi-distributed splitter

Figure 19 shows the periodical BCS-via structure models in even and odd mode. In the even mode, the voltage across each via is zero, therefore no current flows through the vias. The *S*-parameters of the even-mode model is therefore simply the even-mode *S*-parameters of the BCS structure without the vias.

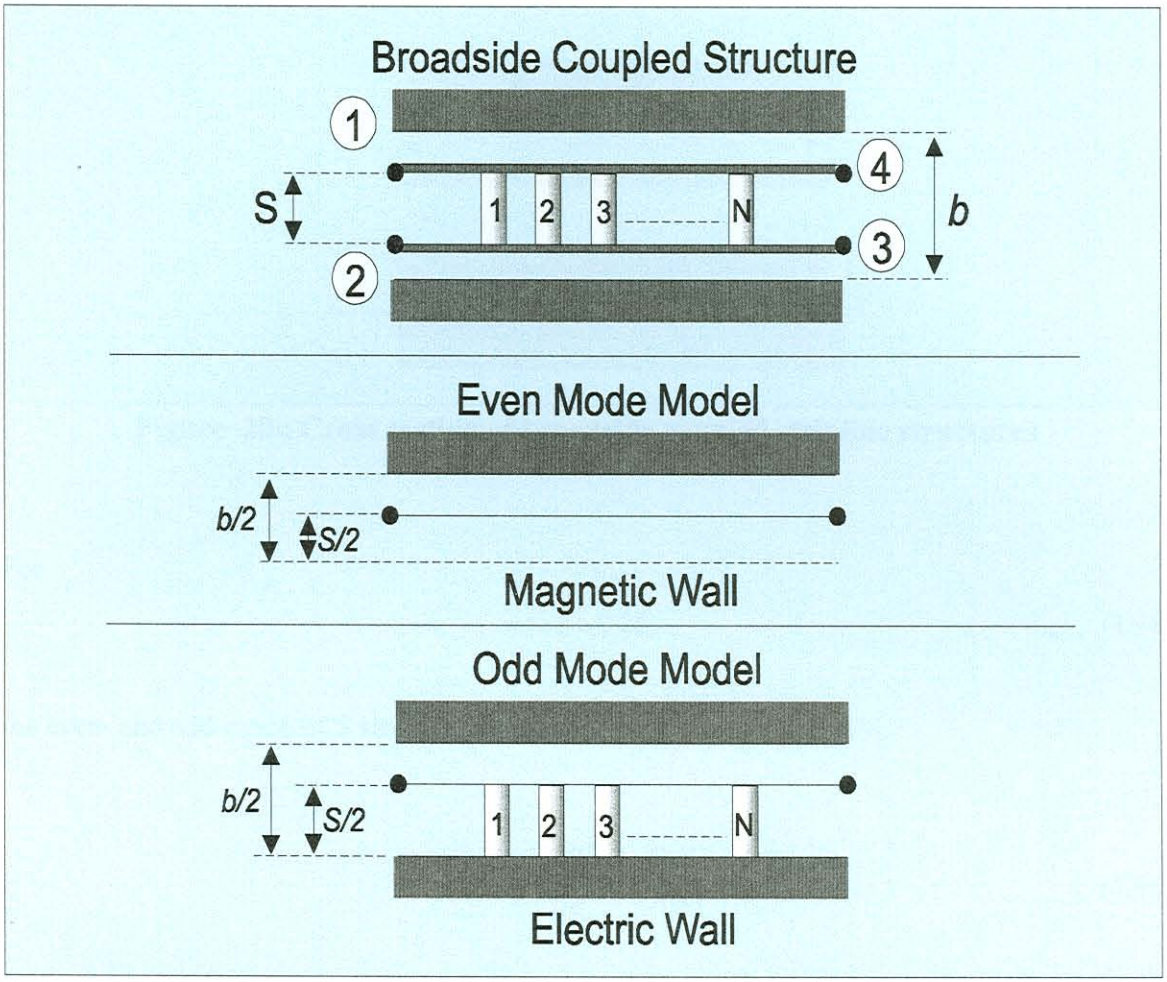

Figure 19 : Even- and odd mode models of the periodical splitter

The structure can be analysed by relating the even- and odd-mode *S*-parameters to the four-port BCS structure *S*-parameters. One port can be terminated in an open circuit load and the 4 port BCS structure *S*-parameters can be reduced to the 3 port splitter *S*-parameters. The splitter can then be evaluated over a broad band for various numbers of vias and via spacings. This investigation will then lead to general design criteria for splitters employed in ultra-wideband coupler-based phase shifters.

3.4.2. Broadside Coupled Stripline Properties

The semi-distributed splitter is realized in homogeneous BCS structure. In this section, the structure properties are discussed. Closed form solutions were published by Cohn [13] for the impedances of BCS structures in homogenious dielectric media. The solutions were presented in terms of complete elliptic integrals *K(k)*, of the first kind. The terminology is clarified in Figure 20.

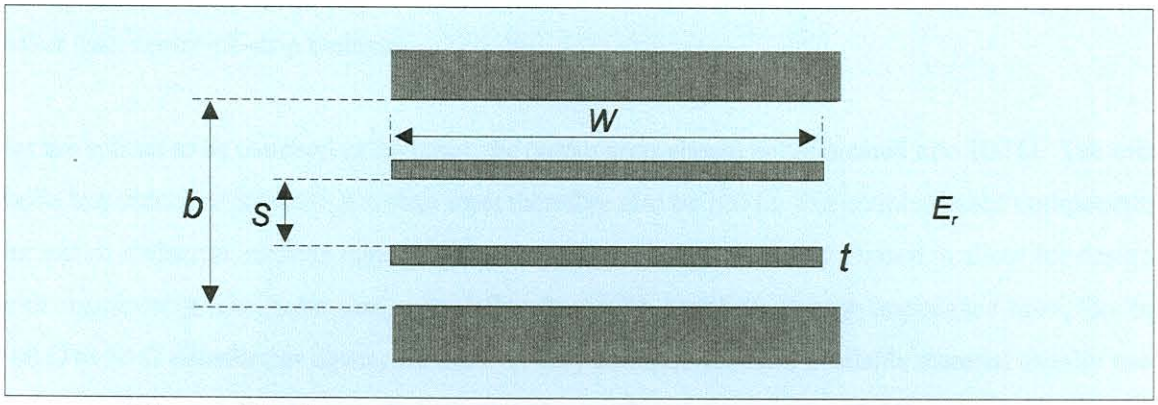

Figure 20 : Cross section of broadside coupled stripline structures

For

$$w/s \geq 0.35, \tag{3.94}$$

the even- and odd-mode BCS stripline impedances are given by Cohn [13].

$$Z_{oe} = \frac{188.3}{\sqrt{\epsilon_r}} \cdot \frac{K(k')}{K(k)} \quad , \tag{3.95}$$

$$Z_{oo} = \frac{296.1}{\sqrt{\epsilon_r} \cdot \frac{b}{s} \tanh^{-1} k} \quad , \tag{3.96}$$

$$k' = \sqrt{1 - k^2} \quad , \tag{3.97}$$

where k is a real number. The normalized strip width is given by

$$w/b = \frac{2}{\pi}\left(\tanh^{-1}\left[\sqrt{\frac{k \cdot \frac{b}{s} - 1}{\frac{1}{k} \cdot \frac{b}{s} - 1}}\right] - \frac{s}{b} \tanh^{-1}\left[\frac{1}{k}\sqrt{\frac{k \cdot \frac{b}{s} - 1}{\frac{1}{k} \cdot \frac{b}{s} - 1}}\right]\right) . \tag{3.98}$$

Cohn [13] found that the finite copper thickness affects the odd-mode impedance the most. For copper thickness less than 1.5 mil, the fringe fields are very close to those of zero thickness.

Normally 0.7 mil (½ ounce copper) is used. Also, s should be taken as the distance between the strips rather than centre-of-strip distance.

For the splitter to be matched to the input, the output arms should be terminated into 100 Ω. The even mode impedance of the BCS-structure must therefore also be 100 Ω. For coupler-based components, the lowest dielectric constant material commercially available is usually chosen to allow for designs with comfortable line dimension, especially where high coupling, or high impedance lines, like the 100 Ω to 50 Ω transformer tapers, are used. A very common standard available material usually used is the PTFE ($\epsilon_r = 2.2$) substrate. Substituting these values into equation (3.95) and solving, we find

$$\frac{K(k')}{K(k)} = 0.7877 \quad , \tag{3.99}$$

and solving for k yields

$$k = 0.8621 \quad . \tag{3.100}$$

Substituting the value of k into equation (3.98), and simplifying, yields

$$Z_{oo} = 153.4 \cdot \frac{s}{b} \quad . \tag{3.101}$$

The designer would then choose s/b and calculate w/b and Z_{oo} using equations (3.98) and (3.101). As an example, a very general choice for a tightly coupled line would be

$$s = 5 \text{ mil} \; ; \; b = 45 \text{ mil}; \quad \epsilon_r = 2.2 \; .$$

Solving equation (3.98) and (3.101) yields:

$$Z_{oo} = 17.0 \; \Omega \quad \text{and} \quad w = 0.602 \text{ mm} \; .$$

Verifying with a full-wave analysis program [14], it is found that

$$w = 0.602 \text{ mm} \; ,$$
$$Z_{oo} = 18.3 \; \Omega \; .$$

It can be concluded that Cohn's closed-form equations [13] are quite accurate and that the equations can be generalized into a more simple form to aid in the design of the semi-distributed splitter.

3.4.3. Via Through-hole Interconnection Properties

In order to accurately analyse the splitter, it is necessary to first analyse the via as an element. This is only needed in the odd-mode analysis, as discussed in 3.4.1. The *S*-parameters of a single via in the odd mode, as in Figure 21, are calculated from 0 to 20 GHz, for various via diameters. A full-wave analysis was used, as described by Jansen [14], which was verified against measurements up to 40 GHz.

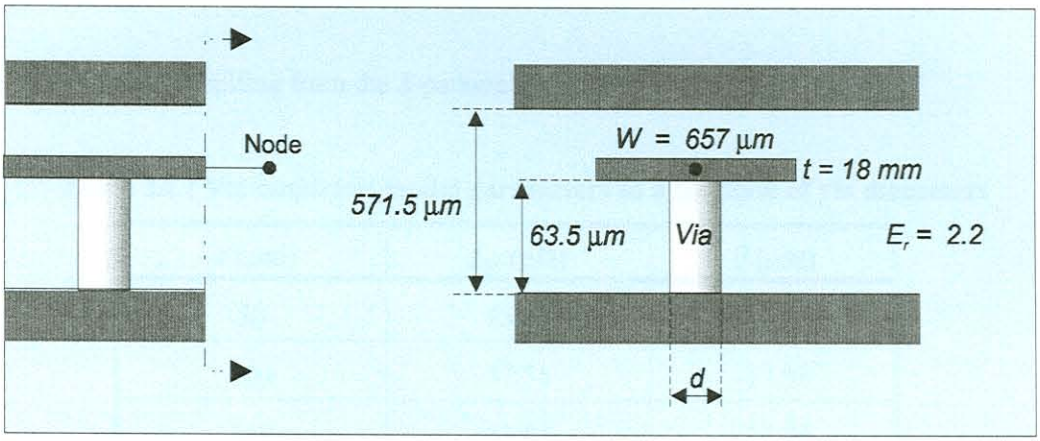

Figure 21 : Odd mode single via full-wave analysis physical structure

It is assumed that the via is perfectly conducting and cylindrical. To analyse the structure, 6 mm line lengths were used to clear the excitation ports from the via. The via model *S*-parameters were printed into a file, for diameters of d = 50, 100, . . . 600 μm from 1 to 20 GHz. The *S*-parameters were de-embedded by 6mm plus half the via diameter. The *S*-parameters were imported into a mathematical CAD program where a model was optimized to fit the *S*-parameters.

After many models were considered, it was found that the *S*-parameters could be very closely fitted to a model comprised of series transmission lines of negative length, and a shunt inductor. The impedance of these lines were chosen to be the same as the BCS structure odd-mode impedance, to allow simple application of the model into the BCS-via structure. The line length can simply be added to the via separation distance, simplifying the BCS-via structure to a length of BCS line, interconnected periodically by inductors. The via empirical model is shown in Figure 22.

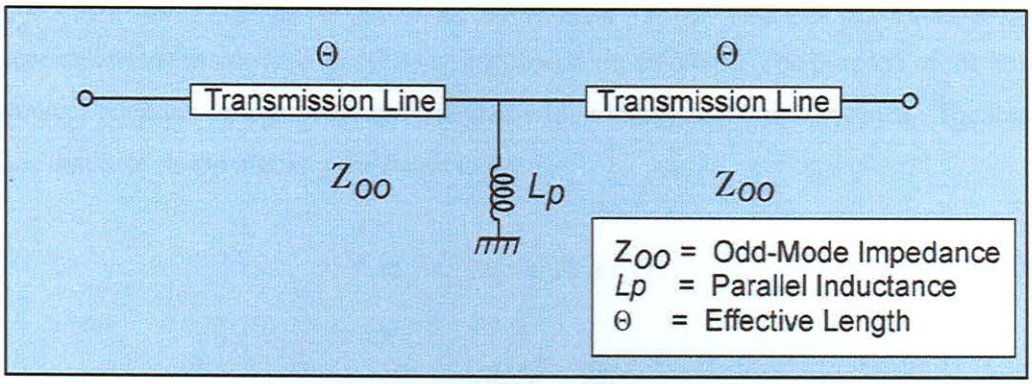

Figure 22 : Odd mode single via empirical model

The element values resulting from the *S*-parameter fit are presented in Table 3.2.

Table 3.2 : Via empirical model parameters as a function of via diameters

d (μm)	*Lp* (pH)	θ (μm)
50	45.64	-13.41
100	37.55	-17.98
150	33.81	-22.46
200	31.41	-26.82
250	30.58	-31.97
300	29.03	-35.72
350	27.44	-39.28
400	27.47	-43.96
450	27.41	-48.55
500	26.99	-52.58
550	26.71	-56.65
600	26.16	-60.42

When compared to the results of the full wave analysis, the *S*-parameters of the equivalent network were found to fit exactly at 0 GHz and about 14 GHz. The worst deviation occurred at about 7 GHz and 20 GHz. The equivalent circuit model reflection coefficient amplitude was a maximum of 0.2 dB higher at 7 GHz and 0.2 dB lower at 20 GHz compared with the full-wave analysis values. The maximum phase difference was 0.5 degrees. It can therefore be concluded that a very accurate model

for the via was found. An empirical equation was derived, with the help of a CAD program, for the inductance and transmission line length as a function of via diameter. The purpose of the empirical mathematical equation is to provide the designer with a handy set of design rules. The empirical equations that best fit the model were found to be

$$L_p = 26.5 + 28\, e^{-8.5d}, \tag{3.102}$$

and

$$\theta = -[855d + 98], \tag{3.103}$$

Where

d represents the via diameter in mm ,
L_p is the shunt inductance in pH ,
θ is the series line length in μm .

The models derived for the via can be used for any 5-mil-spaced BCS structure where the line is wide enough (or the via diameter small enough), to ensure that the via does not interfere with the line fringe field. It was found that the condition was met when

$$w/d > 1.2 . \tag{3.104}$$

These models are accurate to within 1 pH and 7.5 μm. Since this tolerance falls well within the etching material tolerance values, it may be neglected. It can be concluded that an accurate set of empirical equations was derived to assist with the design of ultra-wideband phase shifter splitters.

3.4.4. Semi-Distributed Splitter Odd Mode Analysis

3.4.4.1. Introduction

To simplify the analysis of the splitter, the concept of even and odd mode of operation is utilized, as discussed before. The even-mode analysis is relatively simple because the vias can be excluded from the even-mode model. In the odd-mode analysis, the BCS structure is first assumed to be infinitely long. The reflection and transmission properties of such a structure with a single via interconnection are first determined. The analysis is then extended to a BCS system with n equally spaced vias. It is shown that the structure acts as a filter which resonates under certain conditions, where the odd

mode is not rejected. The criteria to avoid this situation are determined. The general *S*-parameters of the odd mode BCS-via structure are then calculated and discussed.

3.4.4.2. Single-Via Splitter Odd-Mode Properties

The transmission and reflection properties of a single via in BCS, in the odd mode, is derived. The model is shown in Figure 23.

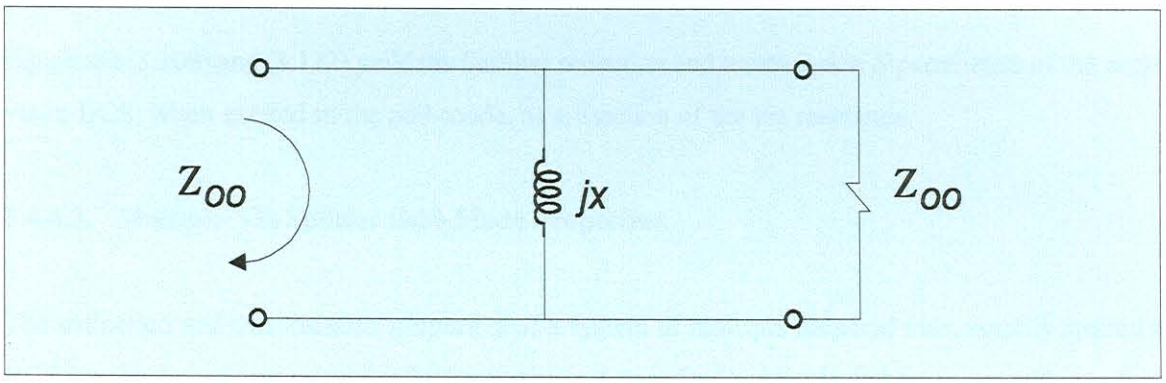

Figure 23 : Odd-mode model of single via in BCS

The transmission line parts of the via model are absorbed in the BCS line, which is chosen to be of the same impedance. The reflection from the via is given by

$$\Gamma = \frac{-1 + 2jx}{1 + 4x^2} \quad , \tag{3.105}$$

where

$$x = \frac{X}{Z_{oo}} \quad . \tag{3.106}$$

For lossless networks, the two general conditions of energy conservation are applied.

$$\sum_{j=1}^{2} | S_{ij} |^2 = 1 \quad , \tag{3.107}$$

$$\sum_{j=1}^{2} S_{jm} \cdot S_{jn}^{*} = 0 \qquad m \neq n \quad . \tag{3.108}$$

Therefore

$$|\Gamma|^2 + |T|^2 = 1 \quad , \tag{3.109}$$

$$\Gamma T^* + T\Gamma^* = 0 \quad , \tag{3.110}$$

$$T = \frac{4x^2 + j\,2x}{1 + 4x^2} \quad , \tag{3.111}$$

$$\therefore \quad T = 1 + \Gamma \quad . \tag{3.112}$$

Equations (3.106) and (3.112) yield the familiar reflection and transmission *S*-parameters of the single via in BCS, when excited in the odd-mode, as a function of the via reactance.

3.4.4.3. Multiple-Via Splitter Odd-Mode Properties

The reflection and transmission properties of a system of multiple identical vias, equally spaced in BCS, can be determined using a reflectogram as in Appendix C. All relevant terms are added to form a mathematical series of terms representing the reflection or transmission coefficient of a n-via system, where $n = 1, 2, 3 \ldots$. Unfortunately the reflectogram complicates rapidly for $n > 3$. The results are as follows:

For a single via ($n = 1$), the reflectogram analysis yields

$$\Gamma_1 = \Gamma \,, \tag{3.113}$$

$$T_1 = T\,\Psi \,. \tag{3.114}$$

For two vias ($n = 2$), the reflectogram analysis yields

$$\Gamma_2 = \Gamma + T^2\,\Psi^2\,\Gamma + T^2\,\Psi^4\,\Gamma^3 + T^2\,\Psi^6\,\Gamma^5 + T^2\,\Psi^8\,\Gamma^7 + \ldots \quad , \tag{3.115}$$

$$= \frac{T^2\,\Psi^2\,\Gamma}{(1 - \Psi^2\,\Gamma^2)} + \Gamma \quad . \tag{3.116}$$

$$T_2 = T^2 \Psi^2 + T^2 \Psi^4 \Gamma^2 + T^2 \Psi^6 \Gamma^4 + T^2 \Psi^8 \Gamma^6 + \ldots \,, \tag{3.117}$$

$$= \frac{T^2 \Psi^2}{(1 - \Gamma^2 \Psi^2)} \,. \tag{3.118}$$

For three vias ($n = 3$), the reflectogram analysis yields

$$\Gamma_3 = \Gamma_2 + \frac{\dfrac{T^4 \Psi^4 \Gamma}{(1 - \Psi^2 \Gamma^2)^3}}{1 - \dfrac{T^2 \Psi^4 \Gamma^2}{(1 - \Psi^2 \Gamma^2)^2}} \,, \tag{3.119}$$

$$T_3 = \frac{\dfrac{T^4 \Psi^4 \Gamma}{(1 - \Psi^2 \Gamma^2)^3}}{1 - \dfrac{T^2 \Psi^4 \Gamma^2}{(1 - \Psi^2 \Gamma^2)^2}} \,. \tag{3.120}$$

Γ, T and Ψ represent the reflection, transmission and phase coefficients of a single via in BCS. It is a simple matter to calculate the close form equations from the infinite series. After much consideration, attempts to write closed-form general equations for a system of n vias from the above results were abandoned, as no arithmetic pattern could be discerned for the results with n as variable. The alternative was to derive a set of recursive equations for the reflection and transmission properties of the general case of n vias in BCS. The reflectogram now consists of only two elements, namely a single via and a set of n vias. The complete reflectogram is shown in Appendix D. The series can be written in closed form as

$$\Gamma_{n+1} = \Gamma + \frac{T^2 \Psi^2 \Gamma_n}{1 - \Gamma \Psi^2 \Gamma_n} \,, \tag{3.121}$$

$$T_{n+1} = \frac{T \Psi T_n}{1 - \Gamma \Psi^2 \Gamma_n} \,. \tag{3.122}$$

It can be shown that these equations can be used iteratively to calculate the S-parameter properties of any number of vias in BCS.

3.4.4.4. Semi-Distributed Splitter Resonance

The semi-distributed splitter has an inherent resonance due to its periodic construction. The splitter application is therefore similar in nature to an odd-mode bandpass filter, used in the rejection frequency band. A typical plot of a BCS-via structure odd-mode transfer characteristic is shown in Figure 24.

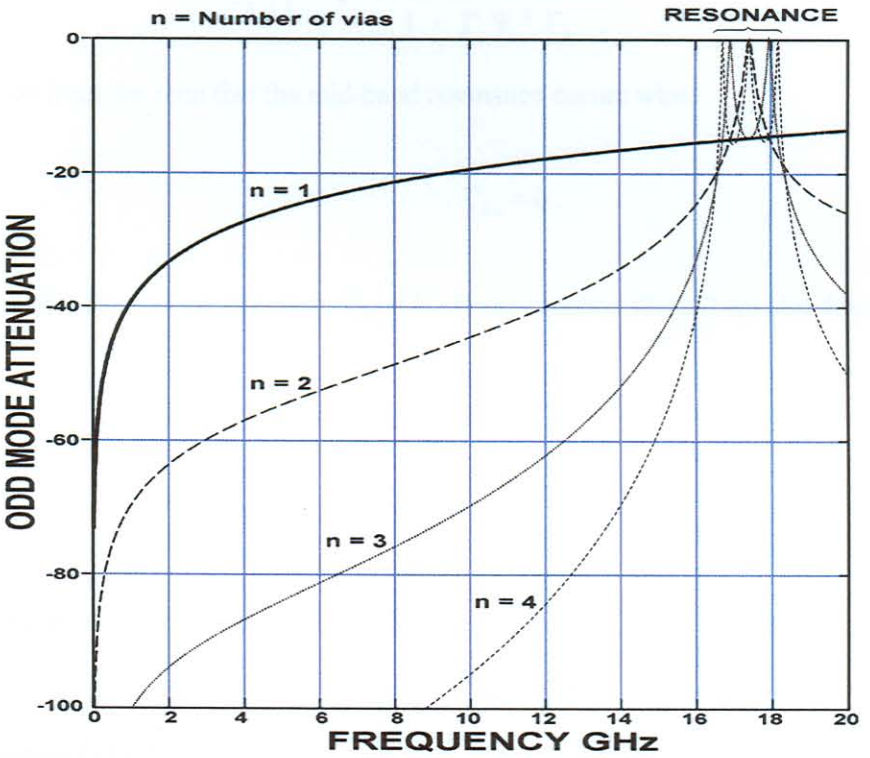

Figure 24 : Odd mode transfer characteristic of the splitter structure

It is clear that, at lower frequencies, the odd mode is rejected, permitting the splitter to be close to ideal. The odd mode causes the twin voltage vectors to be unequal in amplitude and / or phase. At a certain frequency range, the structure resonates or becomes an odd mode passing structure, causing severe splitter imbalance. This frequency band should be avoided. The frequency at which the structure resonates, can be determined in general, when $\Gamma_n = 0$. In graphs of transfer characteristics of BCS-via structures, as shown in Figure 24, it can be seen that exact points of resonance occur when the odd mode attenuation peaks at 0 dB. The graphs peak at the same point at mid-band when

$$\Gamma_k = \Gamma_{k-2} \quad K = 4, 6, 8 \ldots \tag{3.123}$$

Substituting into the equations of section 3.4.4.3, we find the following prediction of resonance. Substitute equation (3.123) into equation (3.121)

$$\Gamma_k = \Gamma + \frac{T^2 \Psi^2 \Gamma_{k-1}}{1 - \Gamma \Psi^2 \Gamma_{k-1}} \quad , \tag{3.124}$$

therefore

$$\Gamma_{k-1} = \Gamma + \frac{T^2 \Psi^2 \Gamma_{k-2}}{1 - \Gamma \Psi^2 \Gamma_{k-2}} \quad . \tag{3.125}$$

From Figure 24 it can be seen that the mid-band resonance occurs when

$$\Gamma_{k-2} = 0 \, . \tag{3.126}$$

From equation (3.125) we conclude that: $\Gamma_{k-1} = \Gamma$. From equation (3.125) we also find, for k even

$$\Gamma_k = 0 \quad , \tag{3.127}$$

and for k odd

$$\Gamma_k = \Gamma \quad . \tag{3.128}$$

Substituting equation (4.124) into (4.126) yields

$$1 + \Psi^2 [T^2 - \Gamma^2] = 0 \quad . \tag{3.129}$$

But from equation (3.112)

$$T = 1 + \Gamma \quad . \tag{3.130}$$

Substituting (3.130) into (3.129) and solving for phase yields

$$\Psi^2 = \frac{-1}{1 + 2\Gamma} \quad . \tag{3.131}$$

For short vias, $x \ll 1$ and $\Gamma \simeq -1$. (3.132)

For example, assume that

$$L_{MAX} = 30pH \quad \text{and} \quad f_{MAX} = 20 \; GHz, \; x \leq 0.2 \quad .$$

Equation (3.105) yields

$$\Gamma = -0.862 + j \; 0.3$$
$$\Gamma \simeq -1 \quad .$$

From equation (3.131), the phase angle between vias at the mid-band resonance condition can be determined from

$$\Psi^2 = \cos 2\theta - j \sin 2\theta \simeq 1 .$$

Therefore

$$\theta = m\,\pi; \qquad m = 1, 2, 3 .... \qquad m \neq 0 . \tag{3.133}$$

Therefore, to avoid the first resonance, the via spacing should be chosen so that, at the highest frequency of operation, $\theta < \pi$. Translating into a simple design guide, we find

$$L_{MAX} = \frac{150}{\sqrt{\epsilon_r}\, f_{MAX}} . \tag{3.134}$$

where L_{MAX} is the maximum via separation in mm and f_{MAX} the frequency, in GHz, when the first resonance occurs.

$$\text{If} \quad \epsilon_r = 2.2 , \quad \text{and} \quad f_{MAX} = 20 \text{ GHz} , \quad \text{then} \quad L_{MAX} = 5.06 \text{ mm} .$$

For the splitter to operate properly at 20 GHz, the via spacing should therefore be considerably less than 5 mm. Typically, a via spacing of 2 or 3 mm is chosen to avoid resonance up to 20GHz.

3.4.5. Semi-Distributed Splitter *S*-parameters

It was demonstrated in section 3.4.1 that the effect of the BCS-coupled structure with n identical equal-spaced via interconnections can be analysed by introducing the well-known even- and odd-mode analysis. The analysis is complicated by the fact that the BCS- via structure *S*-parameters are derived in the odd-mode impedance. These parameters need to be converted to system impedance Z_o at the input and $2Z_o$ at the output ports 3 and 4. The even-mode *S*-parameters can easily be derived in Z_o; $2Z_o$ system-impedance format.

If Γ'_{01}, Γ'_{02} and T'_0 are the input reflection coefficient, output reflection coefficient and transmission *S*-parameters measured in the odd-mode system impedance, it can be shown [15] that these coefficients can be converted to input impedance Z_o at port 1 and 2 and output impedance $2Z_o$ at ports 3 & 4 using the transforms

$$\Gamma_{01} = \frac{(1 - r_0 \Gamma'_{02})(\Gamma'_{01} - r_i) + r_0 (T'_0)^2}{k} , \tag{3.135}$$

$$\Gamma_{02} = \frac{(1 - r_i \Gamma'_{01})(\Gamma'_{02} - r_0) + r_i (T'_0)^2}{k} , \tag{3.136}$$

$$T_0 = \frac{AT'_0}{k} , \tag{3.137}$$

where

$$r_i = \frac{Z_0 - Z_{00}}{Z_0 + Z_{00}} = 0.4641 , \tag{3.138}$$

$$r_o = \frac{2Z_0 - Z_{00}}{2Z_0 + Z_{00}} = 0.6906 , \tag{3.139}$$

$$A = \frac{\sqrt{32}\, Z_0 Z_{00}}{(Z_0 + Z_{00})(2Z_0 + Z_{00})} = 0.6406 , \tag{3.140}$$

$$k = (1 - r_i \Gamma'_{01})(1 - r_o \Gamma'_{02}) - r_i r_0 (T'_0)^2 . \tag{3.141}$$

Using simple energy conservation principles, it can be shown that the even-mode *S*-parameter can be represented by

$$[S_E] = \begin{bmatrix} \Gamma_{E1} & T_E \\ T_E & \Gamma_{E2} \end{bmatrix} = \begin{bmatrix} \frac{1}{3} & \frac{\sqrt{8}}{3} e^{-jn\theta} \\ \frac{\sqrt{8}}{3} e^{-jn\theta} & \frac{-1}{3} e^{-j2n\theta} \end{bmatrix} . \tag{3.142}$$

where $n\theta$ represents the total electrical length of the n sections of θ length of line between the $n + 1$ vias in the four port BCS structure. Using general even- and odd-mode analysis on the four-port BCS structure it can be verified that the scattering parameters $[S']$ are given by

$$S'_{11} = S'_{22} = \frac{\Gamma_{01} + \Gamma_{E1}}{2} = \Gamma_1 \quad , \tag{3.143}$$

$$S'_{33} = S'_{44} = \frac{\Gamma_{02} + \Gamma_{E2}}{2} = \Gamma_2 \quad , \tag{3.144}$$

$$S'_{12} = S'_{21} = \frac{\Gamma_{E1} - \Gamma_{01}}{2} = C_1 \quad , \tag{3.145}$$

$$S'_{43} = S'_{34} = \frac{\Gamma_{E2} - \Gamma_{02}}{2} = C_2 \quad , \tag{3.146}$$

$$S'_{23} = S'_{14} = S'_{41} = S'_{32} = \frac{T_0 + T_E}{2} = T \quad , \tag{3.147}$$

$$S'_{13} = S'_{31} = S'_{24} = S'_{42} = \frac{T_E - T_0}{2} = X \quad . \tag{3.148}$$

The symmetric four-port structure *S*-parameters can be reduced to that of the three port splitter, by leaving one port open, e.g. $b_2 = a_2$ and eliminating b_2.

$$S_{11} = \frac{C_1^2}{(1 - \Gamma_1)} + \Gamma_1 \quad , \tag{3.149}$$

$$S_{22} = \frac{T^2}{(1 - \Gamma_1)} + \Gamma_2 \quad , \tag{3.150}$$

$$S_{33} = \frac{X^2}{(1 - \Gamma_1)} + \Gamma_2 \quad , \tag{3.151}$$

$$S_{12} = S_{21} = \frac{T\,C_1}{(1 - \Gamma_1)} + X \quad , \tag{3.152}$$

$$S_{13} = S_{31} = \frac{X\,C_1}{(1 - \Gamma_1)} + T \quad , \tag{3.153}$$

$$S_{23} = S_{32} = \frac{XT}{(1 - \Gamma_1)} + C_2 \quad . \tag{3.154}$$

Therefore the splitter *S*-parameter matrix can be represented in matrix form as

$$[S] = \begin{bmatrix} \left(\Gamma_\Theta + \frac{C_\Theta^{\,\theta}}{1-\Gamma_\Theta}\right) & \left(X + \frac{TC_\Theta}{1-\Gamma_\Theta}\right) & \left(T + \frac{XC_\Theta}{1-\Gamma_\Theta}\right) \\ \left(X + \frac{TC_\Theta}{1-\Gamma_\Theta}\right) & \left(\Gamma_\theta + \frac{T^\theta}{1-\Gamma_\Theta}\right) & \left(C_\theta + \frac{TX}{1-\Gamma_\Theta}\right) \\ \left(T + \frac{XC_\Theta}{1-\Gamma_\Theta}\right) & \left(C_\theta + \frac{TX}{1-\Gamma_\Theta}\right) & \left(\Gamma_\theta + \frac{X^\theta}{1-\Gamma_\Theta}\right) \end{bmatrix} . \quad (3.155)$$

Port match, transmission loss and amplitude- and phase-match equations were derived and verified against the full-wave analysis. The results were found to be virtually identical from DC to 20GHz.

Device match:

$$S_{\theta\theta} = \Gamma_\Theta + \frac{C_\Theta^{\,\theta}}{1-\Gamma_\Theta} , \quad (3.156)$$

$$S_{\theta\theta} = \Gamma_\theta + \frac{T^\theta}{1-\Gamma_\Theta} , \quad (3.157)$$

$$S_{II} = \Gamma_\theta + \frac{X^\theta}{1-\Gamma_\Theta} . \quad (3.158)$$

Device transfer:

$$S_{\theta\Theta} = X + \frac{TC_\Theta}{1-\Gamma_\Theta} , \quad (3.159)$$

$$S_{I\Theta} = T + \frac{XC_\Theta}{1-\Gamma_\Theta} . \quad (3.160)$$

Device amplitude tracking:

$$\delta_{\hat{a}} = 20 \log \left[\frac{|S_{\theta\Theta}|}{|S_{I\Theta}|}\right] . \quad (3.161)$$

Device phase tracking:

$$ANG_X = Arg \left[\frac{S_{\theta\Theta}}{S_{I\Theta}}\right] . \quad (3.162)$$

3.4.6. Semi-Distributed Splitter Practical Considerations

In realising a test splitter, a 30 micron etching tolerance with very smooth, sharply defined edges could be achieved. The vias could however not be realised satisfactorily by through-hole plating or electro-sputtering techniques, due to their length-to-diameter ratios. Conductive epoxy vias proved to be more capacitive in nature at low frequencies, whereas through-ribbons were found to be more inductive due to the extra length to the point of adhesion. The best vias were realised by a combination of conductive epoxy and ribbons. The splitter is shown in Chapter 5.

The structure resonance for the test splitter was deliberately chosen to be at about 17 GHz, where the theory clearly shows sharp spiky *S*-parameter characteristics as shown in Figure 24. The measured results reveal smoother bump or wavy disturbance due to slight variance in practical via nature and spacing. From the analysis it is apparent that if the via diameter is increased, the odd-mode rejection also increases. However, if the via diameter becomes comparable to the line width, it starts to interfere with the line fringe field, causing even-mode mismatch. A good choice seems to be $d < (w\text{-}s)$. It is also important that the via spacing be close enough so that the circuit will remain far from resonance at the highest operating frequency.

From the *S*-parameter plots of the test splitter it is apparent that the splitter match is virtually independent of via diameter and number. The splitter results are summarised in Table 3.3.

Table 3.3 : Test Splitter Evaluation Results

Parameter	Theory	Practice
S_{11}	Better than -30 dB, rising gradually until resonance	Better than -15 dB up to resonance, about -10 dB at resonance
S_{22}, S_{33}	Within 0.3 dB from -6 dB	Within 0.3 dB from -6 dB
$P\Delta$	Within 0.3 dB up to resonance for all n, improving as n increases	1 via 1.4 dB max @ 20 GHz 2 via 0.6 dB max @ 20 GHz 3 via 0.4 dB max @ 20 GHz
$\Delta\phi$	4.2° at 20 GHz for single via, 2° max up to resonance for $n > 1$	1 via 7.5° max @ 20 GHz 2 via 5° max @ 20 GHz 3 via 3° max @ 20 GHz

From the sensitivity analysis and the results in table 3.3, it is clear that the phase imbalance is the most compelling reason to implement multiple vias. Referring to the sensitivity analysis in Chapter 4, these results will typically cause phase and amplitude errors for a 45° phase shifter constructed from the tandem connection of two couplers, as in table 3.4.

Table 3.4 : Predicted Phase Shifter Tolerance due to Splitter Tolerance

n	Phase Error	Amplitude Error	Phase Shift Deviation	Loss Deviation
1 via	7.5 Deg	1.4 dB	0.8 Deg	0.2 dB
2 vias	5 Deg	0.6 dB	0.3 Deg	0.04 dB
3 vias	3 Deg	0.4 dB	0.2 Deg	0.03 dB

3.5. Conclusion

The three elements comprising the phase shifter were analysed in depth. A general impedance transformer was developed in the form of an impedance-transforming tapered line, to best conserve symmetry. It was concluded that these tapers are relatively immune against material variations. The coupler design was then discussed at length and the tolerance analysis of stripline couplers was discussed. It was found that the rotational alignment of stripline couplers is critical to the symmetry of the device. Both the phase and amplitude characteristics are shown to be important for the performance of the phase shifter. A critical element to the phase shifter is the splitter. From the sensitivity analysis it follows that the signal should be split into equal amplitude and phase vectors. An ultra-wideband splitting structure was developed to split incoming signals into twin vectors. It has been demonstrated mathematically, and verified in practise, that for a splitter with close spacing of three or more through-vias, very good results can be obtained. The splitting amplitude and phase balance are virtually independent of BCS line width tolerances and via nature, as long as resonance is avoided.

References

[1] K. C. Gupta, R. Garg, and R. Chadha, "Computer aided design of microwave circuits", Artech House, Massachusetts, 1981.

[2] J. A. G. Malherbe, "Microwave transmission line filters", Artech House, Massachusetts, 1980.

[3] W. J. Getsinger, "Coupled rectangular bars between parallel plates", IRE Trans. MTT, vol. MTT-10, no. 1, pp. 65-72, Jan. 1972.

[4] R. E. Collin, "Foundations for microwave engineering", McGraw-Hill, New York, 1966.

[5] R. W. Klopfenstein, "A transmission line taper of improved design", IRE Proc., vol. 44, pp. 31-35, Jan. 1956.

[6] R. P. Hecken, "A near-optimum matching section without discontinuities", IEEE Trans. Microwave Theory Tech., vol. 20, pp. 734-739, Nov. 1972.

[7] E. G. Crystal and L. Young, "Theory and tables of optimum symmetric TEM-mode coupled-transmission-line directional couplers", IEEE Trans Microwave Theory Tech., vol. 13, no. 5, pp 544-558, Sept. 1965.

[8] C. P. Tresselt, "The design and construction of broadband high-directivity, 90-degree couplers using non-uniform line techniques", IEEE Trans Microwave Theory Tech., vol. 14, no. 12, pp. 647-656, Dec. 1966.

[9] D. W. Kammler, "The design of discrete N-section and continuously tapered symmetrical microwave TEM directional couplers ", IEEE Trans Microwave Theory Tech., vol. 17, no. 8, pp. 577-589, Aug. 1969.

[10] J. P. Shelton and J. A. Mosko, "Synthesis and design of wide-band equal-ripple TEM directional couplers and fixed phase shifters", IEEE Trans Microwave Theory Tech., vol. MTT-14, pp. 462-473, Oct. 1966.

[11] D. Srigiripuram, Shamasundara, and K. C. Gupta, "Sensitivity analysis of coupled microstrip directional couplers ", IEEE Trans Microwave Theory Tech., vol. 26, no. 10, pp. 788-794, Oct. 1978.

[12] F. V. Minnaar, J. C. Coetzee, and J. Joubert, "The development of an ultra-wideband via connected broadside coupled splitting structure", in IEEE AP MTT - Symp., Cape Town, S.A., pp. 465 - 466, Sept 1998.

[13] S. B. Cohn, "Characteristic impedances of broadside-coupled strip transmission lines", IRE Trans. Microwave theory Tech., vol. MTT-8, no. 6, pp. 633-647, Nov. 1960.

[14] R. H. Jansen, "A full-wave electromagnetic model of cylindrical and conical via hole grounds for use in interactive MIC/MMIC design", Proc. of the IEEE International Symposium, pp. 1233-1236, Albuquerque, USA, June 1992.

[15] K. Kurokana, "Generalized 2-port scattering parameters for arbitrary load and generator impedances", IEEE Trans Microwave Theory Tech., pp. 194, March 1965.